

Effect of Borehole Deviation on Breakout Orientations

LARRY MASTIN

Department of Applied Sciences, Stanford University, Stanford, California

Well bore breakouts are zones of spalling and fracture that form on opposite sides of a well bore and tend to change the cross-sectional shape of the borehole from circular to roughly elliptical. In vertical holes drilled in areas where one principal stress (S_v) is vertical, breakouts tend to form at opposite ends of the borehole diameter parallel to the least compressive horizontal principal stress direction (S_h). This paper uses an analytical elastic solution for stress at the wall of a borehole to analyze the rotation of breakout orientations away from the direction of S_h as the borehole deviates from the direction of the vertical principal stress. The calculated orientations of breakouts in deviated boreholes depend on the type of faulting regime in which the well was drilled (i.e., normal, strike-slip, or thrust), on the deviation angle ϕ of the borehole axis from vertical, on the angle θ between the horizontal projection of the borehole axis and the direction of S_h , and on the relative magnitudes of the three principal stresses (S_h ; S_H , the greatest compressive horizontal stress; and S_v). In the strike-slip faulting regime, regardless of the values of θ , S_v , S_H , and S_h , a borehole must deviate at least 35° from vertical before the horizontal projection of the breakout orientation differs by more than 10° from S_h . In the normal and thrust faulting regimes, however, the borehole deviation angle ϕ_{crit} required to rotate projected breakout orientations by 10° from S_h approaches zero as the value of S_h approaches that of S_H . In the thrust faulting regime, only about 3% of all combinations of θ , S_v , S_H , and S_h will produce ϕ_{crit} values less than 10° , while about 12% of all such combinations will yield $\phi_{crit} < 10^\circ$ in the normal faulting regime. About 12% and 33% of such combinations will yield $\phi_{crit} < 20^\circ$ in the thrust and normal faulting regimes, respectively. Careful study of changes in breakout orientation as a function of borehole deviation may improve the resolution of inferred stress directions when studying breakouts in deviated boreholes in these two faulting regimes.

INTRODUCTION

Since the early 1980s, when well bore breakouts became widely used as an indicator of regional stress orientations, our understanding of regional stress patterns has advanced dramatically. In the United States alone the data base for stress orientations has increased by more than 75% since *Zoback and Zoback's* [1980] compilation, largely due to the contribution of breakout data [*Zoback and Zoback*, 1988]. In areas of the world where the stress state was previously unknown, breakout data are beginning to define relatively detailed stress patterns [*Zoback*, 1987].

Breakouts are zones of spalling and fracture on opposite sides of a well bore, which elongate it in cross section from circular to approximately elliptical (Figure 1). Breakouts generally form by compressive failure of the rock at the borehole wall and tend to occur at the azimuth along the well bore where the compressive stress is greatest. If the borehole axis coincides with one of the principal stress directions, elastic theory [*Jaeger and Cook*, 1979; p. 251] predicts that the most compressive stress at the borehole wall exists at the azimuth parallel to the least compressive remote stress that acts perpendicular to the borehole axis. Within 1 or 2 km of the Earth's surface, in areas of low topographic relief, one of the principal stresses is generally considered to be vertical. Thus breakouts in vertical boreholes are inferred to form parallel to the least compressive remote horizontal stress (S_h , Figure 1). Numerous comparisons with other stress direction indicators [e.g., *Zoback et al.*, 1987; *Bell and Gough*, 1983; *Hickman et al.*, 1985; *Plumb and Cox*, 1987] show that this inference is generally valid for breakouts in vertical holes.

If, however, the borehole deviates from vertical, or extends to great depth, or is drilled in an area with significant topographic relief, breakout orientations are related in a complex way to the relative magnitudes of all three principal stresses, and their orientations relative to that of the borehole. Because few boreholes are exactly parallel to one of the principal stress directions, it becomes important to ask how far a borehole must deviate from one of the principal stress directions before breakout orientations depart significantly from the simple theoretical relationship given above. In this paper we use an analytical solution for elastic stress to determine breakout directions in an arbitrarily oriented borehole, in a stress field consisting of horizontal and vertical remote principal stresses.

METHOD OF SOLUTION

Fairhurst [1968] has derived analytical expressions for the stress at the wall of a uniformly loaded borehole of arbitrary

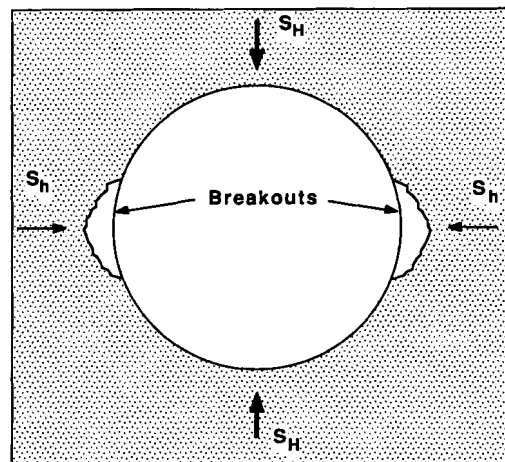


Fig. 1. Schematic cross section of a borehole containing breakouts.

Copyright 1988 by the American Geophysical Union.

Paper number 8B2111.
0148-0227/88/008B-2111\$05.00

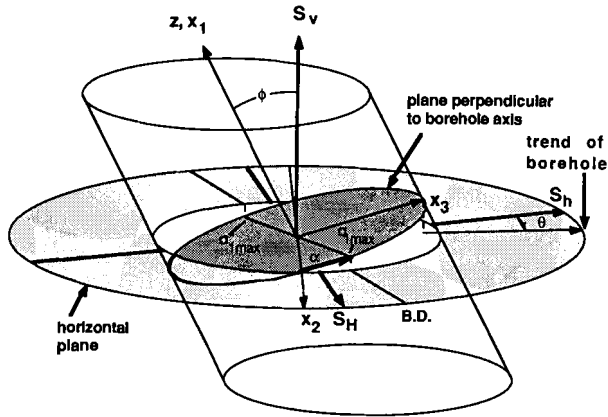


Fig. 2. Illustration of the breakout orientation projected onto the horizontal plane (B.D.) and the values ϕ and θ , which describe the borehole orientation relative to the principal stress directions S_v , S_H , and S_h . Breakouts are inferred to form at the location of the greatest compressive stress (σ_{1max}). The local Cartesian coordinates x_1 , x_2 , and x_3 and the local cylindrical coordinates z and α are used in the Fairhurst [1968] equations for stress (Appendix A). The x_3 coordinate is oriented upward in the plane perpendicular to the borehole axis. Thus the projection of the x_3 axis onto the horizontal plane represents the trend of the borehole axis in the horizontal plane, and the angle between this projected orientation and the direction of S_h is the value θ .

orientation relative to the principal stress directions. The equations employed by Fairhurst assume an isotropic, homogeneous, linearly elastic medium, with equal and constant fluid pressures in the well bore and the surrounding material (Appendix A). For specified remote stresses and borehole orientations these solutions were used to determine the azimuth of the greatest compressive stress, σ_{1max} , at the borehole wall,

the azimuth at which breakouts are inferred to form. For simplicity, the principal stress directions (S_H , S_h , and S_v) are assumed to be vertical and horizontal (Figure 2). The inferred breakout orientations were calculated throughout a range of values of S_H , S_h , S_v , and borehole orientation to understand how these variables control breakout orientation.

RESULTS

The effect of borehole deviation on breakout orientations varies significantly between the thrust faulting regime (where the vertical stress S_v is the least compressive stress), the strike-slip faulting regime (where S_v is the intermediate stress), and the normal faulting regime (where S_v is the greatest compressive stress). It is important to note that the study of an inclined borehole in one of these regimes represents a specific case of the general problem of a borehole in an arbitrarily oriented stress field. In effect, by treating each of these three stress regimes separately, we are looking at the same general stress state from three perpendicular directions.

The most useful method for illustrating the pattern of breakout directions as a function of borehole orientation is a lower hemisphere, equal-angle stereographic projection (Figure 3a). Each tick mark on this plot represents an inferred breakout orientation (i.e., the orientation of σ_{1max}), projected onto a horizontal plane, for a particular borehole orientation (relative to S_h , S_H , and S_v). The azimuthal position of the tick represents the trend of the horizontal projection of the borehole, measured in degrees (θ , Figure 2) from the direction of S_h . The radial position of the tick represents the deviation angle ϕ in degrees from vertical.

Breakout orientations are most commonly determined from unprocessed dipmeter logs or from the logs of borehole televiewers. Because Schlumberger low-angle dipmeter logs (used

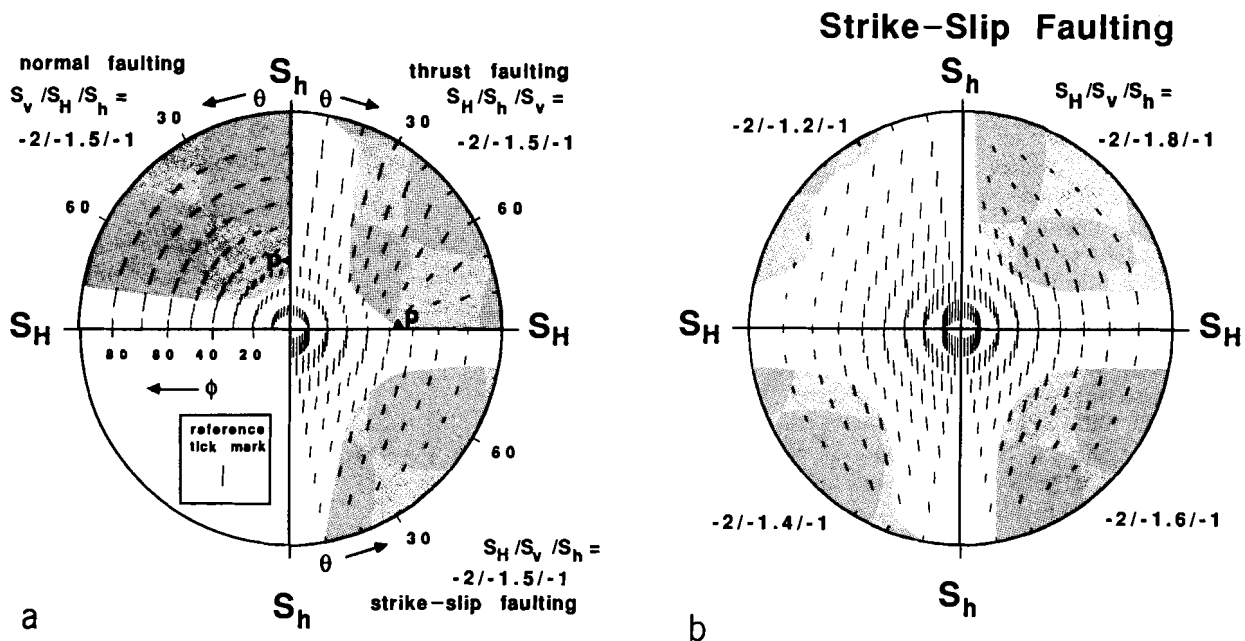


Fig. 3. (a) Stereographic projection of breakout orientations, projected onto a horizontal plane, for a variety of borehole orientations in the normal faulting (upper left quadrant), thrust faulting (upper right quadrant) and strike-slip faulting (lower right quadrant) regimes. The shaded regions include all borehole orientations in which the projected breakout orientations differ from that of S_h by 10° or more. The length of each tick mark is proportional to the square root of the stress anisotropy $(\sigma_{1max} - \sigma_{1min})/\sigma_{1min}$. A reference tick mark is shown whose length corresponds to $(\sigma_{1max} - \sigma_{1min})/\sigma_{1min} = 4$. (b) Stereographic projection of breakout orientations for four values of $S_H/S_v/S_h$ in the strike-slip faulting regime. (c) Stereographic projection of breakout orientations for four values of $S_H/S_h/S_v$ in the thrust faulting regime. (d) Stereographic projection of breakout orientations for four values of $S_v/S_H/S_h$ in the normal faulting regime.

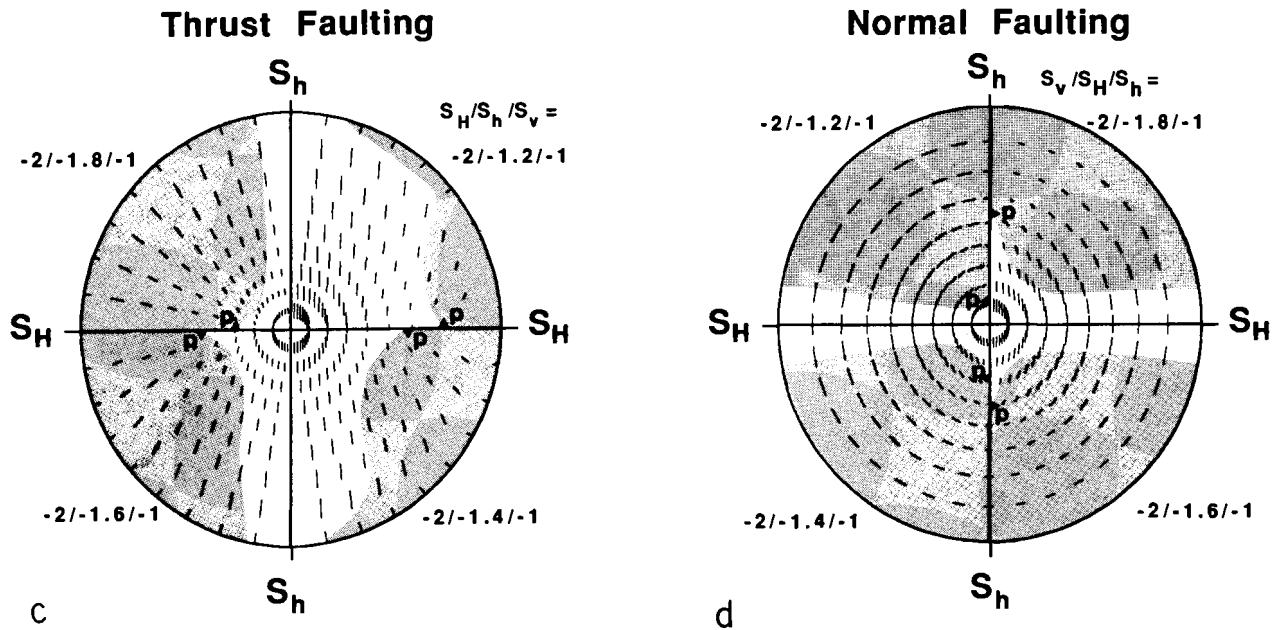


Fig. 3. (continued)

in boreholes which deviate less than 36° from vertical) give the orientations of the caliper arms, relative to magnetic north, projected onto a horizontal plane, the breakout projections in Figure 3 can be compared directly with those from low-angle dipmeter surveys. Schlumberger high-angle dipmeter logs (used in borehole that deviate 36° – 72° from vertical) give orientations of features relative to the high side of the hole, which can be compared with orientations in Figure 3 after some conversion. Dipmeter tools determine orientations using a three-axis magnetometer and thus determine orientations reliably regardless of the hole deviation. Borehole televiwers, on the other hand, determine orientations using a single flux gate magnetometer [Zemanek et al., 1970]. The orientation of features determined by televiwers in deviated boreholes may

differ greatly from their true direction relative to magnetic north due to measurement errors introduced by the tool (Appendix B). However, if the orientation of the borehole with respect to magnetic north is known, these errors can be corrected.

The pattern of breakout orientations in Figure 3a is distinct from one faulting regime to another. In the normal faulting regime (upper left quadrant), for all θ , breakouts approach an orientation parallel to the horizontal azimuth in the borehole (i.e., parallel to the x_2 direction, Figure 2), producing a more or less concentric pattern on the stereonet. In the thrust faulting regime (upper right, Figure 3a), breakouts approach an orientation perpendicular to the horizontal azimuth in the borehole, producing a radial breakout pattern on the stereonet. In the strike-slip faulting regime (lower right, Figure 3a), in boreholes trending subparallel to S_h , breakouts have a radial

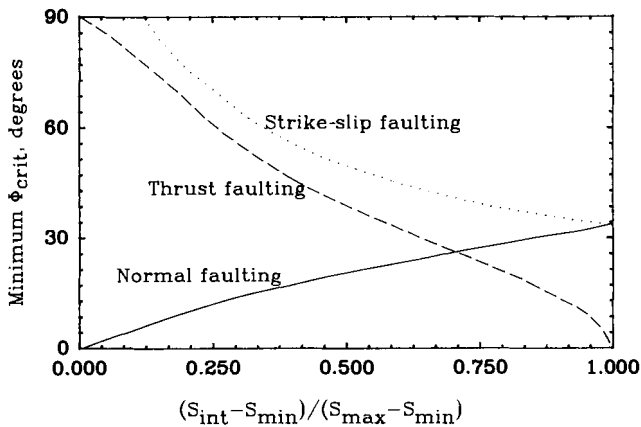


Fig. 4. Minimum values of ϕ_{crit} for all values of θ , as a function of the stress ratio $(S_{int} - S_{min}) / (S_{max} - S_{min})$ for the strike-slip faulting regime (dotted curve), thrust faulting regime (dashed curve), and normal faulting regime (solid curve). The values S_{max} , S_{int} , and S_{min} are the greatest compressive, intermediate, and least compressive principal stresses, respectively. Thus $(S_{int} - S_{min}) / (S_{max} - S_{min}) = (S_H - S_h) / (S_v - S_h)$ in the normal faulting regime, $(S_h - S_v) / (S_H - S_v)$ in the thrust faulting regime, and $(S_v - S_h) / (S_H - S_h)$ in the strike-slip faulting regime.

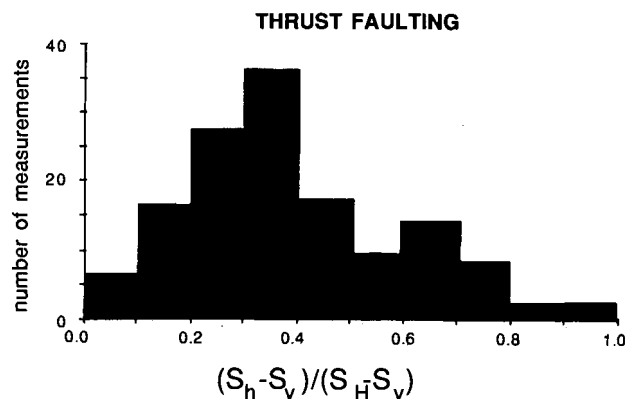


Fig. 5. Histograms of stress ratios calculated from 127 published in situ stress measurements, including those compiled by McGarr and Gay [1978], and others presented by Bredehoeft et al. [1976], Zoback et al. [1980], Zoback and Hickman [1982], Rummel et al. [1983], Tsukahara [1983], Schnapp et al. [1983], Ljunggren and Raillard [1987], Haimson [1982], and Rougiers et al. [1982].

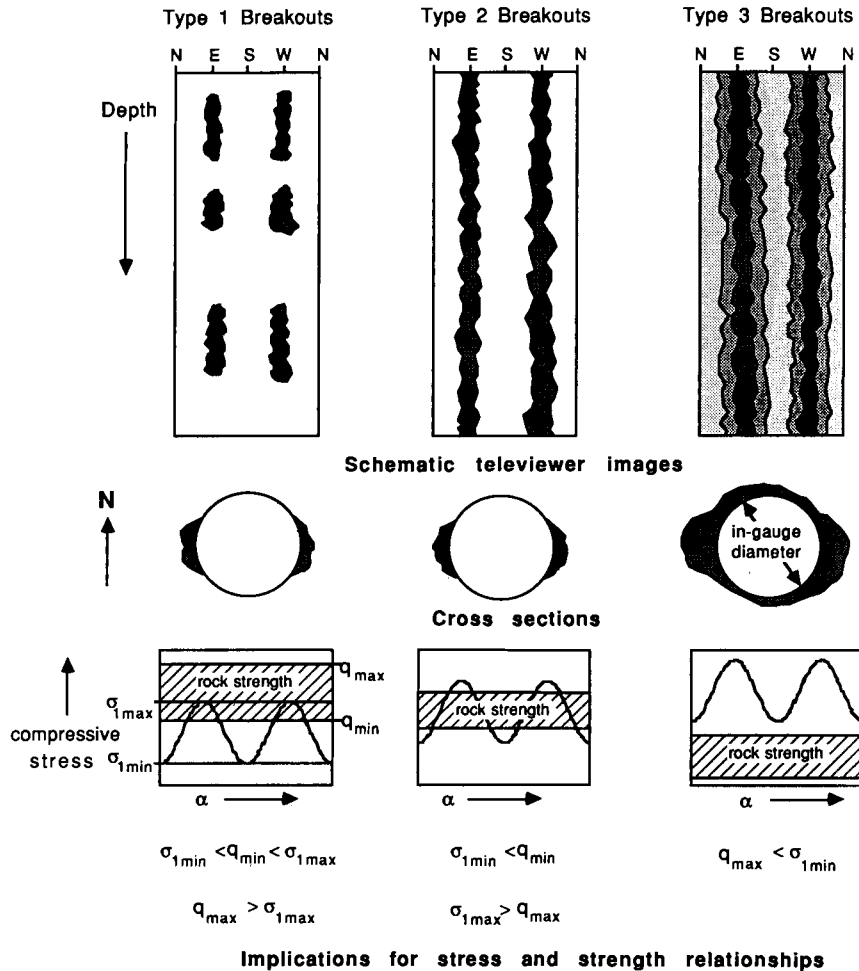


Fig. 6. Schematic illustration of characteristics of type 1, type 2, and type 3 breakouts. (Top) Schematic patterns of types 1, 2, and 3 breakouts as they might appear in a televiewer log. These logs show surface features on a borehole wall as a function of azimuth relative to magnetic north (horizontal scale) and depth (vertical scale). Spalled regions are represented by a stippled pattern, while intact sections are unstippled. Breakouts are represented as pairs of dark vertical stripes which occur 180° from one another on the televiewer logs. (Middle) Schematic cross sections of type 1, type 2, and type 3 breakouts. (Bottom) Relationships between the relative values of σ_{1max} , σ_{1min} , q_{max} , and q_{min} implied by type 1, type 2, and type 3 breakouts. The inequalities “<” and “>” indicate “less compressive than” and “more compressive than.”

orientation, while those in boreholes trending subparallel to S_H have a concentric orientation.

The shaded regions in Figure 3a show the domain of borehole orientations where projected breakout orientations differ by more than 10° from the direction of S_h . One can obtain the critical deviation ϕ_{crit} required to enter the shaded region for a particular borehole orientation θ by following a radial line out from the center of the plot. In all cases, the lowest values of ϕ_{crit} occur at values of θ which are intermediate between 0° and 90°. For boreholes that deviate in the plane perpendicular to either the most or least compressive principal stress, ϕ_{crit} is undefined because the breakout orientations do not rotate with increasing ϕ . However, for boreholes that deviate in the plane perpendicular to the intermediate principal stress, breakout orientations change abruptly at the direction labeled P. Near P, breakout orientations vary rapidly with borehole orientation, and the stress is nearly isotropic at the borehole wall. The nearly isotropic stress state around P also makes it unlikely that consistently oriented breakouts will form in this region (unless breakout orientations are controlled by rock anisotropy).

In each faulting regime the size of the shaded region varies with the relative magnitudes of the three principal stresses, particularly the magnitude of the intermediate principal stress S_{int} relative to the most and least compressive stresses S_{max} and S_{min} , respectively. In the strike-slip faulting regime, for example (Figure 3b), where $S_{int} = S_v$, the size of the shaded region increases, and the average value of ϕ_{crit} for a given θ decreases, as S_v approaches S_H in magnitude (going counterclockwise from the upper left). In the thrust faulting regime (Figure 3c) and the normal faulting regime (Figure 3d) the size of the shaded region increases as S_H approaches S_h in magnitude (clockwise from upper right). Interestingly, the orientation P, where σ_1 is nearly isotropic, migrates toward vertical as S_H approaches S_h . If S_H were equal to S_h , P would be vertical; all breakout orientations would be perfectly concentric about the center of the plot in the normal faulting regime, and radial about the center of the plot in the thrust faulting regime.

The minimum value of ϕ_{crit} for all values of θ (i.e., the minimum distance ϕ on the stereonet between the shaded region and the origin) is plotted in Figure 4 as a function of

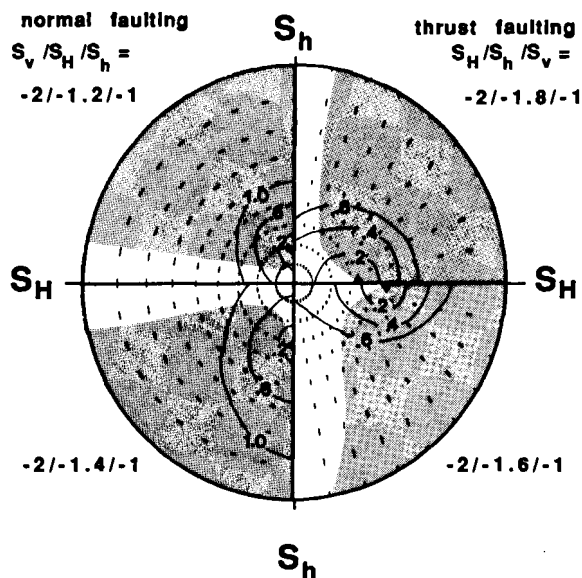


Fig. 7. Stereonet giving breakout orientations for two states of stress in the normal faulting (left side) and thrust faulting (right side) regimes. Contours are plotted for values of $(\sigma_{1max} - \sigma_{1min})/\sigma_{1min}$. The shaded regions indicate borehole orientations where breakouts differ by more than 10° from S_h . Small triangles indicate the orientation P.

the stress ratio $(S_{int} - S_{min})/(S_{max} - S_{min})$. In the strike-slip faulting regime, $\phi_{crit} > 34^\circ$ for all stress ratios. In contrast, in both the normal and thrust faulting regimes, ϕ_{crit} goes to zero as S_h approaches S_H in magnitude (in the normal faulting regime this corresponds to a stress ratio of zero, whereas in the thrust faulting regime it corresponds to a stress ratio of 1). Throughout the domain of stress ratios in the normal faulting regime, minimum values of ϕ_{crit} are less than 35° .

DISCUSSION AND ROCK STRENGTH CONSIDERATIONS

It should be emphasized that breakout orientations in deviated boreholes depend on factors (specifically, θ and the principal stress magnitudes) that are not well constrained in most breakout studies. Given a typical case where ϕ is known but θ and the principal stress magnitudes are not, one cannot determine a priori whether breakout orientations in a particular borehole will be significantly rotated or not. In such a case, assuming that all possible combinations of θ and the stress ratio $(S_{int} - S_{min})/(S_{max} - S_{min})$ are equally likely, one can estimate the likelihood that breakout orientations are rotated by calculating the percentage of such combinations that produce a significant rotation in breakout orientations. In the thrust faulting regime, for example, only 3% of all combinations of θ and the stress ratio give $\phi_{crit} < 10^\circ$, while 12% of all such combinations yield $\phi_{crit} < 10^\circ$ in the normal faulting regime. Thus a borehole which deviates 10° from vertical in a normal faulting regime will have approximately a 12% chance of producing breakouts which are rotated by 10° or more from S_h . For a borehole deviation of 20° the probabilities increase to 12% in the thrust faulting regime and 33% in the normal faulting regime, respectively.

These probabilities hinge on the assumption that all values of the stress ratio are equally likely. A compilation of 127 stress measurements from thrust faulting regimes in North America, Europe, Africa, and Asia (Figure 5) suggests that stress ratios approaching 1.0 in the thrust faulting regime may

be less common than lower stress ratios. Published stress measurements from normal faulting regimes are too sparse for a similar compilation to be meaningful.

The problem of determining ϕ_{crit} with no knowledge of θ or the stress ratio is made more complicated, but perhaps less problematic, by the fact that the stress anisotropy in subvertical boreholes approaches zero as ϕ_{crit} approaches zero. In Figure 3 the length of each tick mark is proportional to the square root of the stress anisotropy $(\sigma_{1max} - \sigma_{1min})/\sigma_{1min}$, where σ_{1min} is the least compressive stress calculated at the borehole wall, generally located at the azimuth perpendicular to σ_{1max} . (A square root relationship is used instead of a linear relationship in order to make the tick mark orientations more visible where $(\sigma_{1max} - \sigma_{1min})/\sigma_{1min}$ is small.) In each faulting regime the stress anisotropy is greatest in holes oriented parallel to the intermediate principal stress direction, and is least at the orientation P.

With some knowledge of rock strength and some inferences about stress anisotropy in a particular borehole, it may be possible to constrain the values of θ and the stress ratio. For example, the presence of continuous, consistently oriented breakouts throughout a depth interval suggests that the greatest compressive stress at the borehole wall (σ_{1max}) exceeded the rock strength everywhere in that interval, while (to a first approximation) a lack of failure at the azimuth perpendicular to the breakouts suggests that σ_{1min} is less than the rock strength everywhere. If the strength q of a rock unit in a depth interval ranges between certain bounds (q_{min} and q_{max}), the existence of breakouts with these characteristics requires that $\sigma_{1min} < q_{min} < q_{max} < \sigma_{1max}$. Such breakouts are illustrated schematically in the center column of Figure 6 and are referred to as type 2 breakouts, to distinguish them from breakouts which occur sporadically with depth ("type 1" breakouts; left side, Figure 6) and breakouts which extend around the entire perimeter of the wellbore ("type 3" breakouts; right side, Figure 6).

Because the existence of type 2 breakouts suggests that $\sigma_{1min} < q_{min} < q_{max} < \sigma_{1max}$, we deduce that $(\sigma_{1max} - \sigma_{1min})/\sigma_{1min}$ must be greater than $(q_{max} - q_{min})/q_{min}$. In Figure 7, values of $(\sigma_{1max} - \sigma_{1min})/\sigma_{1min}$ are contoured on stereonet plots for two specific cases each of normal and thrust faulting. In essence, these contour lines circumscribe regions around the orientation P inside of which type 2 breakouts will not form for a given value of $(q_{max} - q_{min})/q_{min}$. If type 2 breakouts are observed over some interval in a well and q_{max} and q_{min} are known for that interval, then the borehole orientation must lie outside of the contours equal to $(q_{max} - q_{min})/q_{min}$. In such circumstances it may be possible to constrain the relative values of S_H , S_h , and S_v (as outlined, for example, by Zoback et al. [1986] and perhaps to eliminate from the realm of possibility certain stress ratios which give low values of ϕ_{crit}).

CONCLUSIONS

In the strike-slip faulting regime, because of the insensitivity of breakout orientations, breakout studies need not be restricted to vertical or nearly vertical boreholes. Breakouts in boreholes that deviate up to 30° from vertical will theoretically give orientations that are within 10° of S_h . In the normal and thrust faulting regimes, subequal horizontal stresses may cause significant changes in breakout orientation even in boreholes that deviate less than 10° from vertical. Subequal horizontal stresses may be indicated in some circumstances by lack of type 2 breakouts or by inconsistent or widely varying

stress direction indicators. If subequal horizontal stresses are indicated, it may be possible to improve the resolution of inferred stress directions by compiling data only from the most nearly vertical sections of boreholes. The major benefit of such work would be to improve our ability to resolve stress directions from breakouts.

APPENDIX A: USE OF THE FAIRHURST EQUATIONS TO DETERMINE BREAKOUT ORIENTATIONS

The equations for stress at the wall of an arbitrarily oriented borehole are [Fairhurst, 1968]

$$\sigma_{zz} = S_{11} - 2\nu(S_{22} - S_{33}) \cos 2\alpha + 4\nu S_{23} \sin 2\alpha \quad (A1)$$

$$\sigma_{\alpha\alpha} = S_{22} + S_{33} - \nu(S_{22} - S_{33}) \cos 2\alpha + 4S_{23} \sin 2\alpha \quad (A2)$$

$$\tau_{z\alpha} = 2(S_{13} \cos \alpha - S_{12} \sin \alpha) \quad (A3)$$

The stresses at the borehole wall in these equations (σ_{zz} , $\sigma_{\alpha\alpha}$, $\tau_{z\alpha}$; Figure A1) are given in in local cylindrical coordinates of the well bore, z and α , where z is oriented parallel to the borehole axis in the upward direction and α is the angle around the well bore in the plane perpendicular to the borehole axis, measured counterclockwise from the x_2 direction (Figure 2). The variables S_{ij} are remote effective stresses (Figure A1), given in the right-handed Cartesian coordinate system x_i where x_1 lies along the borehole axis (upward being positive), x_2 is oriented horizontally in the plane perpendicular to the borehole axis, and x_3 is directed upward, perpendicular to x_1 and x_2 , in the plane perpendicular to the borehole axis (Figure 2). The principal stress directions (assumed to be vertical and horizontal here) form a right-handed coordinate system in which the vertical stress (S_v , Figure 2) is positive in the upward direction. The principal stress directions are related to x_1 , x_2 , and x_3 by ϕ , the angle between the $+S_v$ direction and the $+x_1$ direction, and θ , the angle measured counterclockwise from the $+S_h$ direction to the horizontal projection of the $+x_3$ axis onto the horizontal plane (Figure 2). The convention for positive shear and normal stresses is shown in Figure A1.

When ϕ and θ equal zero, the above equations reduce to

$$\sigma_{zz} = S_v - 2\nu(S_H - S_h) \cos 2\alpha \quad (A4)$$

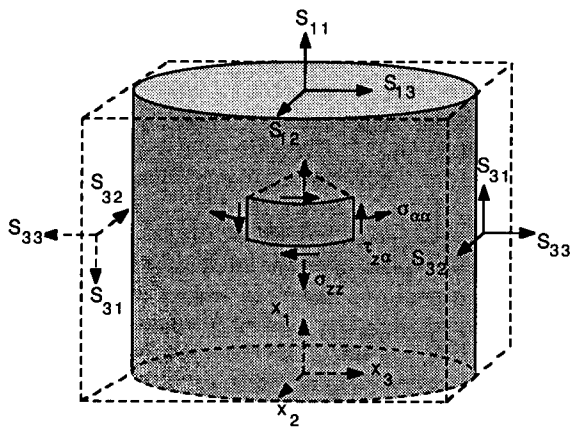


Fig. A1. Illustration of the conventions for positive stress ($\sigma_{\alpha\alpha}$, σ_{zz} , $\tau_{z\alpha}$) around a well bore, in local cylindrical coordinates (z and α), and positive stresses (S_{11} , S_{22} , S_{33} , S_{12} , S_{23} , S_{13}) in the local Cartesian x_1 - x_2 - x_3 coordinate system.

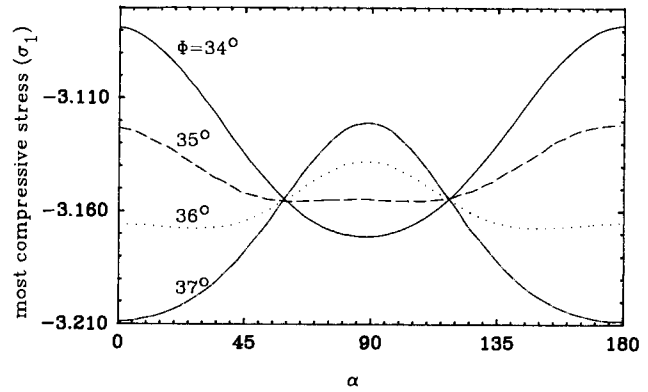


Fig. A2. σ_1 versus α for four different borehole orientations near P in the normal faulting regime for the stress conditions illustrated in Figure 3a. $\theta = 90^\circ$ for each curve.

$$\sigma_{\alpha\alpha} = S_H + S_h - 2(S_H - S_h) \cos 2\alpha \quad (A5)$$

$$\tau_{\alpha\alpha} = 0 \quad (A6)$$

Equation (A5) is identical to the Kirsch [1898] solution for elastic stress at a borehole wall due to plane strain loading [Jaeger and Cook, 1979, p. 251]. In vertical holes the stresses σ_{zz} and $\sigma_{\alpha\alpha}$ at the borehole wall are both principal stresses. They are most compressive at the azimuth of S_h , thereby producing breakouts at that orientation. Where the borehole axis does not coincide with S_v , $\tau_{z\alpha}$ is not necessarily equal to zero; that is, the principal stresses on the wall of the hole are not necessarily parallel or perpendicular to the borehole axis. The greatest compressive principal stress σ_1 at a point on the borehole wall is given by

$$\sigma_1 = 0.5\{\sigma_{zz} + \sigma_{\alpha\alpha} - [(\sigma_{zz} - \sigma_{\alpha\alpha})^2 + 4\tau_{z\alpha}^2]^{1/2}\} \quad (A7)$$

Unlike the values of $\sigma_{\alpha\alpha}$ and σ_{zz} derived from the Kirsch solution, σ_1 is not necessarily sinusoidal as a function of α , although it is periodic with a period of π (Figure A2). The σ_1 versus α curve departs from a sinusoidal pattern primarily for borehole orientations in the vicinity of the orientations P, illustrated in Figure 3. In those regions, σ_1 approaches an isotropic state around the borehole wall.

The above equations assume that the fluid pressure in the well bore is equal to the pore pressure in the surrounding rock. An excess fluid pressure in the well bore would superimpose a tension on $\sigma_{\alpha\alpha}$ but would not affect σ_{zz} or $\tau_{z\alpha}$ [Aadnoy and Chenevert, 1987]. Thus an increase in the fluid pressure in the well bore would tend to rotate principal stresses on the borehole wall toward orientations that are parallel and perpendicular to the borehole axis. Such a fluid pressure could also cause the location of the greatest compressive stress (σ_{1max}) to move toward the azimuth on the well bore where $\sigma_{\alpha\alpha}$, as given in (A2), is most compressive. These effects are not considered here.

APPENDIX B: DETERMINATION OF ORIENTATIONS FROM TELEVIEWER LOGS IN DEVIATED BOREHOLES

Breakouts are currently studied using two kinds of instruments: the four-arm caliper, which is usually part of a high-resolution dipmeter of the kind used by Schlumberger, and an acoustic borehole televiewer, which provides an acoustic image of features on the borehole wall. The dipmeter uses a three-axis magnetometer which detects the three-dimensional

in the horizontal plane. The radial distance from the center of the plot corresponds to the deviation of the borehole from vertical (ϕ). The length of each tick mark is proportional to the strength of the component of the magnetic field vector in the plane perpendicular to the borehole axis. The magnetic north vector (whose orientation is indicated by the solid triangle) is inclined 65° down from horizontal.

orientation of the magnetic north vector and allows the orientations of features on the borehole wall to be accurately measured.

The orientation of features in a borehole televiewer log are determined using a single flux gate magnetometer which is attached to the rotating mechanism in the televiewer and triggers once during each revolution at the azimuth where the Earth's magnetic field interacts most strongly with the flux gate elements [Zemanek *et al.*, 1970]. In vertical boreholes the magnetometer triggers on the magnetic north direction, which is the projection of the magnetic north vector onto the horizontal plane. In deviated boreholes the magnetometer triggers at the orientation given by the projection of the magnetic north vector onto the plane perpendicular to the borehole axis. When this projected orientation is projected again onto the horizontal plane, it may differ significantly from the true magnetic north direction in the horizontal plane.

Figure B1 shows a stereonet plot of the horizontal projection of the magnetic north direction triggered by a televiewer flux gate magnetometer, as a function of borehole orientation. The inclination of the magnetic north vector in this plot (solid triangle) is 65° down from horizontal, which is within the typical range of 60° – 70° for the conterminous United States [Dobrin, 1976, p. 488]. The projected orientations differ significantly from the true direction of magnetic north throughout much of the domain of borehole orientations. However, if the orientation of a borehole with respect to magnetic north is known, the true orientation of the trigger pulse can be calculated. Table B1 gives rough correction values for the horizontal projection of the trigger pulse orientation in boreholes which deviate up to 40° from vertical, for magnetic inclinations of 60° and 70° .

35	-121.38	-154.59
40	-137.73	-157.37
	$\theta = 20^\circ$	
5	-3.62	-6.24
10	-9.07	-17.76
15	-17.62	-40.96
20	-31.39	-78.85
25	-52.41	-109.35
30	-77.53	-124.80
35	-98.18	-132.62
40	-111.39	-136.89
	$\theta = 30^\circ$	
5	-5.19	-8.84
10	-12.60	-23.49
15	-23.13	-46.38
20	-37.41	-73.31
25	-54.52	-94.29
30	-71.36	-107.20
35	-84.96	-114.84
40	-94.58	-119.38
	$\theta = 40^\circ$	
5	-6.51	-10.94
10	-15.20	-26.98
15	-26.33	-47.52
20	-39.45	-67.82
25	-53.04	-83.36
30	-65.27	-93.74
35	-75.00	-100.40
40	-82.11	-104.57
	$\theta = 50^\circ$	
5	-7.53	-12.47
10	-16.87	-28.66
15	-27.72	-46.49
20	-39.18	-62.38
25	-50.03	-74.39
30	-59.28	-82.73
35	-66.53	-88.29
40	-71.84	-91.86
	$\theta = 60^\circ$	
5	-8.23	-13.43
10	-17.71	-29.00
15	-27.79	-44.28
20	-37.57	-57.01
25	-46.27	-66.54
30	-53.41	-73.25

TABLE B1. (continued)

ϕ , deg	Error in MN, deg	
	$\gamma = 60^\circ$	$\gamma = 70^\circ$
	$\theta = 60^\circ$ (continued)	
35	-58.91	-77.81
40	-62.86	-80.74
	$\theta = 70^\circ$	
5	-8.63	-13.87
10	-17.84	-28.36
15	-26.91	-41.37
20	-35.16	-51.73
25	-42.15	-59.38
30	-47.71	-64.80
35	-51.87	-68.48
40	-54.76	-70.80
	$\theta = 80^\circ$	
5	-8.72	-13.85
10	-17.39	-27.02
15	-25.39	-38.06
20	-32.27	-46.54
25	-37.87	-52.73
30	-42.18	-57.09
35	-45.30	-60.02
40	-47.33	-61.79
	$\theta = 90^\circ$	
5	-8.55	-13.42
10	-16.50	-25.17
15	-23.41	-34.48
20	-29.10	-41.45
25	-33.56	-46.46
30	-36.87	-49.95
35	-39.14	-52.24
40	-40.46	-53.53
	$\theta = 100^\circ$	
5	-8.14	-12.65
10	-15.26	-22.95
15	-21.14	-30.76
20	-25.79	-36.46
25	-29.30	-40.51
30	-31.79	-43.27
35	-33.37	-45.02
40	-34.11	-45.90
	$\theta = 110^\circ$	
5	-7.53	-11.59
10	-13.75	-20.46
15	-18.67	-26.95
20	-22.42	-31.59
25	-25.14	-34.82
30	-26.97	-36.99
35	-27.99	-38.28
40	-28.27	-38.83
	$\theta = 120^\circ$	
5	-6.75	-10.31
10	-12.05	-17.79
15	-16.09	-23.10
20	-19.06	-26.82
25	-21.12	-29.38
30	-22.41	-31.04
35	-23.00	-31.97
40	-22.93	-32.25
	$\theta = 130^\circ$	
5	-5.82	-8.85
10	-10.21	-14.98
15	-13.43	-19.23
20	-15.73	-22.16
25	-17.26	-24.14
30	-18.13	-25.38
35	-18.40	-26.02
40	-18.09	-26.12

TABLE B1. (continued)

ϕ , deg	Error in MN, deg	
	$\gamma = 60^\circ$	$\gamma = 70^\circ$
	$\theta = 140^\circ$	
5	-4.78	-7.24
10	-8.26	-12.08
15	-10.75	-15.36
20	-12.47	-17.60
25	-13.56	-19.08
30	-14.11	-19.98
35	-14.17	-20.40
40	-13.73	-20.37
	$\theta = 150^\circ$	
5	-3.66	-5.52
10	-6.25	-9.11
15	-8.06	-11.51
20	-9.27	-13.12
25	-10.01	-14.17
30	-10.34	-14.79
35	-10.28	-15.05
40	-9.83	-14.96
	$\theta = 160^\circ$	
5	-2.47	-3.72
10	-4.19	-6.09
15	-5.37	-7.66
20	-6.14	-8.71
25	-6.60	-9.38
30	-6.77	-9.77
35	-6.68	-9.91
40	-6.31	-9.82
	$\theta = 170^\circ$	
5	-1.25	-1.87
10	-2.10	-3.05
15	-2.68	-3.83
20	-3.06	-4.34
25	-3.27	-4.67
30	-3.35	-4.85
35	-3.28	-4.92
40	-3.08	-4.86

The parameter γ is the inclination of the magnetic north vector in degrees down from horizontal. For $\theta = 0^\circ$ to -180° (not shown in this table), the error in the magnetic north orientation is the negative of the error for a corresponding borehole of the same ϕ value and the negative of the θ value.

Acknowledgments. The initial work on this problem was funded by the Geophysics Institute, University of Karlsruhe, West Germany. Additional work was paid for by the Stanford Rock and Borehole Geophysics Program. Peter Blümling, Thomas Schneider, and Birgit Claus in Karlsruhe provided a great deal of assistance in the early stages of the project. Helpful reviews of this paper were made by Jim Springer, Colleen Barton, Jon Olson, and Joann Stock. Tough but constructive criticisms by Steve Hickman and Brian Evans have improved this paper considerably.

REFERENCES

- Aadnoy, B. S., and M. E. Chenevert, Stability of highly inclined boreholes, *SPE Drill. Eng.*, 2, 364-374, 1987.
- Bell, J. S., and D. I. Gough, The use of borehole breakouts in the study of crustal stress, in *Hydraulic Fracturing Stress Measurements*, edited by M. D. Zoback and B. C. Haimson, pp. 201-209, National Academy Press, Washington, D. C., 1983.
- Bredehoeft, J. D., R. G. Wolff, W. S. Keys, and E. Shuter, Hydraulic fracturing to determine the regional in situ stress field, Piceance Basin, Colorado, *Geol. Soc. Am. Bull.*, 87, 250-258, 1976.
- Dobrin, M. B., *Introduction to Geophysical Prospecting*, 3rd ed., 630 pp., McGraw-Hill, New York, 1976.

- Fairhurst, C., Methods of determining in situ rock stresses at great depths, *Tech. Rep. TRI-68*, Mo. River Div. Corps of Eng., Omaha, Nebr., 1968.
- Gay, N. C., Fracture growth around openings in thick-walled cylinders of rock subjected to hydrostatic compression, *Int. J. Rock Mech. Min. Sci. Geomech. Abstr.*, 10, 209-233, 1973.
- Haimson, B. C., Comparing hydrofracturing deep measurements with overcoring near-surface tests in three quarries in western Ohio, *Proc. U.S. Symp. Rock Mech.*, 23rd, 190-202, 1982.
- Hickman, S. H., J. H. Healy, and M. D. Zoback, In situ stress, natural fracture distribution, and borehole elongation in the Auburn geothermal well, Auburn, New York, *J. Geophys. Res.*, 90, 5497-5512, 1985.
- Jaeger, J. C., and N. G. W. Cook, *Fundamentals of Rock Mechanics*, 3rd ed., 593 pp., Chapman and Hall, New York, 1979.
- Kirsch, G., Die Theorie der Elastizität und die Bedürfnisse der Festigkeitslehre, *VDI Z*, 42, 707, 1898.
- Ljunggren, C., and G. Raillard, Rock stress measurements by means of hydraulic tests on pre-existing fractures at Gideå test site, Sweden, *Int. J. Rock Mech. Min. Sci. Geomech. Abstr.*, 24, 339-346, 1987.
- McGarr, A., and N. C. Gay, State of stress in the Earth's crust, *Annu. Rev. Earth Planet. Sci.*, 6, 405-436, 1978.
- Plumb, R. A., and J. W. Cox, Stress directions in eastern North America determined to 4.5 km from borehole elongation measurements, *J. Geophys. Res.*, 92, 4805-4816, 1987.
- Rougiers, J.-C., J. D. McLennan, and L. D. Schultz, In situ stress determinations in northeastern Ohio, *Proc. U.S. Symp. Rock Mech.*, 23rd, 219-229, 1982.
- Rummel, F., J. Baumgärtner, and H. J. Alheid, Hydraulic fracturing stress measurements along the eastern boundary of the SW-German block, in *Hydraulic Fracturing Stress Measurements*, edited by M. D. Zoback and B. C. Haimson, pp. 3-17, National Academy Press, Washington, D. C., 1983.
- Schnapp, M. J., J. G. Kocherhans, and R. A. Nelson, Stress measurements in salt in a deep borehole, southeastern Utah, in *Hydraulic Fracturing Stress Measurements*, edited by M. D. Zoback and B. C. Haimson, pp. 79-85, National Academy Press, Washington, D. C., 1983.
- Tsukahara, H., Stress measurements utilizing the hydraulic fracturing technique in the Kanto-Tokai area, Japan, in *Hydraulic Fracturing Stress Measurements*, edited by M. D. Zoback and B. C. Haimson, pp. 18-27, National Academy Press, Washington, D. C., 1983.
- Zemanek, J. E., E. Glen, Jr., L. J. Norton, and R. L. Cardwell, Formation evaluation by inspection with the borehole televiewer, *Geophysics*, 35, 254-269, 1970.
- Zoback, M. D., and S. Hickman, In situ study of the physical mechanisms controlling induced seismicity at Monticello Reservoir, South Carolina, *J. Geophys. Res.*, 87, 6959-6974, 1982.
- Zoback, M. D., H. Tsukahara, and S. Hickman, Stress measurements at depth in the vicinity of the San Andreas fault: Implications for the magnitude of shear stress at depth, *J. Geophys. Res.*, 85, 6157-6173, 1980.
- Zoback, M. D., L. G. Mastin, and C. Barton, In situ stress measurements in deep boreholes using hydraulic fracturing, well bore breakouts, and stonely wave polarization, in *Rock Stress and Rock Stress Measurements*, edited by O. Stefansson, pp. 289-300, Centek Publishers, Luleå, Sweden, 1986.
- Zoback, M. D., et al., New evidence on the state of stress of the San Andreas fault system, *Science*, 238, 1105-1111, 1987.
- Zoback, M. L., Global pattern of intraplate tectonic stresses, *Eos Trans. AGU*, 68, 1209-1210, 1987.
- Zoback, M. L., and M. D. Zoback, State of stress in the conterminous United States, *J. Geophys. Res.*, 85, 6113-6156, 1980.
- Zoback, M. L., and M. D. Zoback, Tectonic stress field of the continental United States, Geophysical Framework of the Continental United States, edited by L. C. Pakiser and W. D. Mooney, *Mem. Geol. Soc. Am.*, in press, 1988.

L. Mastin, Department of Applied Sciences, Stanford University, Stanford, CA 94305.

(Received February 10, 1988;
revised April 14, 1988;
accepted March 23, 1988.)